# Effect of Wind-Duration, Swell-Contamination, and Bimodal Ocean Wave Spectra on Acoustic Doppler

Richard S. Keiffer
Naval Research Laboratory
Stennis Space Center, MS 39529 USA

*Abstract* - **The purpose of the this paper is to apply a new time domain scattering model [1] (not limited to small wave heights, small slopes, or plane waves) to developing seas which may be swell-contaminated and which assume a new bimodal ocean wave directionality function [2]. This attribute of the directionality of the ocean waves is generated through nonlinear wave-wave interaction in which energy near the spectral peak feeds into both, shorter and longer wavelength components. The goal in this paper is to use these new models to further refine current estimations for the magnitude and Doppler characteristics of the acoustic scattering from the sea surface. It is hoped that these revised estimates can be used by other researchers trying to determine the characteristics of other scattering mechanisms expected to be active in the near-surface region of the sea surface.**

## I. INTRODUCTION

The purpose of the this paper is to apply a new time domain scattering model [1] (not limited to small wave heights, small slopes, or plane waves) to developing seas which may be swell-contaminated and which assume a new bimodal ocean wave directionality function [2]. More specifically, a bimodal distribution of the first kind is generated through nonlinear wave-wave interaction in which energy near the spectral peak feeds into both, shorter and longer wavelength components. The goal in this paper is to use these new models to further refine current estimations for the magnitude and Doppler characteristics of the interface backscattering component of acoustic reverberation from the sea surface. These revised estimates for the contribution that the interface scattering makes to received frequency spectrum can then be used by other researchers as a new benchmarks from which refined estimates can be derived for other scattering mechanisms expected to be active in the near-surface region of the sea surface.

Although the frequency shifting and broadening of acoustic signals backscattered from the sea surface has been the subject of many studies, important aspects of the physics driving this problem remain unclear due to a variety of modeling and experimental difficulties. The problem is particularly interesting and complex in the low to moderate frequency regime (less than about 3 kHz) because air bubbles, injected into the near-surface region by breaking waves, may significantly influence the magnitude and possibly the spectrum of the scattered signal through two different competing mechanisms [3]. Also, a detailed knowledge of the ocean wave spectrum at the time of an at-sea experiment is usually lacking so acoustic modelers often adopt canonical parameterizations for the ocean wave field. In some cases, these descriptions result in misleading acoustic predictions but, more generally, they simply do not support the detailed analysis needed to differentiate between different near-surface scattering mechanisms. Finally, most acoustic measurements involve moving resources. While the Doppler effects due to uniform rectilinear motion of the source and/or receiver can be "subtracted out" leaving only the frequency scattering due to the moving air/sea interface and other scatterers (e. g., fish, bubble clouds) near the ocean surface, this is an idealization that requires further scrutiny. For example, the undulating motion experienced by a source or receiver array as it is pulled through the water will cause frequency modulation effects that tend to smear out the Doppler spectrum. Although typically not estimated at all, this system induced spreading of the reverberation frequency spectrum may become as large as the expected Doppler shifts due to scattering from the air/sea interface and obviously cannot simply be subtracted out. A reasonable approach to sorting out the various components of the problem is to accurately model one of the phenomena involved and assign any discrepancy with the data to other mechanisms. When scattering from fish can be ruled out, the surface scattering component is usually modeled and the environmental parameters needed to drive bubble scattering models have been inferred. This seems to be a necessary "bootstrapping" process considering the experimental difficulties of characterizing the dynamic near surface region at sub-wavelength scales.

## II. MODELING MIXED OCEAN SURFACES AND BIMODAL DIRECTIONALITY

The common situation encountered in practical sonar applications is a "mixed sea" or "swell-contaminated sea", composed of a remotely generated wave field and a locally generated wave system. These mixed seas are produced either by distant storms or by rotating winds. A mixed sea may have a double peak in its frequency spectrum. The study of wind-driven seas, swell, and

This work has been supported by the U. S. Naval Research through the U. S. Naval Research Laboratory, Program Element No. 61153N-32, and by grants of computer time at the DoD High Performance Computing Shared Resource Center located at Stennis Space Center, MS.

# Report Documentation Page

*Form Approved*
*OMB No. 0704-0188*



| 1. REPORT DATE | 2. REPORT TYPE | 3. DATES COVERED |
|---|---|---|
| **SEP 2008** | | **00-00-2008 to 00-00-2008** |

| 4. TITLE AND SUBTITLE | 5a. CONTRACT NUMBER |
|---|---|
| **Effect of Wind-Duration, Swell-Contamination, and Bimodal Ocean Wave Spectra on Acoustic Doppler** | 5b. GRANT NUMBER |
| | 5c. PROGRAM ELEMENT NUMBER |
| 6. AUTHOR(S) | 5d. PROJECT NUMBER |
| | 5e. TASK NUMBER |
| | 5f. WORK UNIT NUMBER |
| 7. PERFORMING ORGANIZATION NAME(S) AND ADDRESS(ES) **Naval Research Laboratory,Stennis Space Center,MS,39529** | 8. PERFORMING ORGANIZATION REPORT NUMBER |
| 9. SPONSORING/MONITORING AGENCY NAME(S) AND ADDRESS(ES) | 10. SPONSOR/MONITOR'S ACRONYM(S) |
| | 11. SPONSOR/MONITOR'S REPORT NUMBER(S) |

12. DISTRIBUTION/AVAILABILITY STATEMENT
**Approved for public release; distribution unlimited**

13. SUPPLEMENTARY NOTES
**See also ADM002176. Presented at the MTS/IEEE Oceans 2008 Conference and Exhibition held in Quebec City, Canada on 15-18 September 2008.**

14. ABSTRACT
**see report**

15. SUBJECT TERMS

| 16. SECURITY CLASSIFICATION OF: | | | 17. LIMITATION OF ABSTRACT | 18. NUMBER OF PAGES | 19a. NAME OF RESPONSIBLE PERSON |
|---|---|---|---|---|---|
| a. REPORT **unclassified** | b. ABSTRACT **unclassified** | c. THIS PAGE **unclassified** | **Same as Report (SAR)** | **10** | |

their interaction has been the subject of many investigations and an exhaustive review of the pertinent literature is beyond the scope of this paper. The goal of this section is to set forth basic criteria for discussing and modeling deterministic time-evolving realizations that are representative of mixed sea states for the purpose of simulating the acoustic backscattered response.

*A. Mixed Seas*

There exists no universal or absolute criterion to distinguish sea from swell and the terminology itself is not standardized. Often, sea is defined as the component driven by the local wind, and everything else is taken as swell. In analyzing records of wave measurements, a separation frequency ( $F_S$ ) is usually defined to facilitate the distinction [4]. Wave components with frequencies higher than $F_S$ are assumed to be largely due to the local wind and wave components having frequencies lower than $F_S$ are associated with swell. One practical way to estimate the separation frequency is to assume that the spectral components of the locally wind-generated sea have their phase velocity less than or equal to the local wind speed. Therefore, the separation frequency is the frequency at which the phase velocity equals the local wind speed. This concept suggests that the local sea cannot contribute to the lowest frequency (longest wave) part of the spectrum of the mixed sea. On the other hand, when the wind ceases or changes directions, the high frequency components of the spectrum are the first to disappear. From numerical modeling, it appears that components of the wave field having frequencies higher than about 1. 25 times the peak frequency (i.e., the frequency where the ocean wave frequency spectrum is maximum) disappear quickly [5] when the winds change. Assuming that the swell originates from a fully-developed sea characterized by a Pierson-Moskowitz (PM) spectrum [6], the peak frequency is, $F_{PM}^{peak} = 0.128 g / u_{10}^{swell}$ , where $g$ is the acceleration due to gravity and $u_{10}^{swell}$ is the wind speed at 10 m height (of the previous or distant wave system that will become the swell). In this case, the separation frequency places a high frequency limit on contributions that the swell can make to the mixed sea wave spectrum, $F_{swell} < 1.25 \cdot F_{PM}^{peak} = 0.16\, g / u_{10}^{swell}$ .

A review of the literature on the subject of sea surfaces containing wind-driven seas and swell shows the following: (a) High frequencies components of a wind-driven sea arise first but they are also the first to disappear when wind ceases or turns. (b) The swell, once generated, can propagate huge distances apparently with little or no attenuation [5]. (c) Clear evidence from field measurements of swell interacting with wind-wave development is lacking [5]. Although in principle, short wind-driven wave components can be suppressed by the presence of long waves (swell), the effect is too small to be observed at sea [7]. Another interesting observation from numerical modeling is that the coupling between wind-wave and swell spectra decreases as the angular separation between the directional spectra increases. For angular separations larger than 90˚ there is no coupling at any frequency. In the case of a rotating wind, for rotations less than 90˚, the entire spectrum rotates very rapidly (< 1 hr). For rotations larger than 90˚ a new sea develops while the old sea gradually decays [5]. On the other hand, some hybrid wave models (e. g. , GONO, NOWAMO) make the assumption that the spectral components of swell propagate without loss or interaction through a local wind-driven sea, provided they are more energetic than the corresponding spectral components of the sea [8]. Those swell components that are less energetic than the corresponding spectral components of the sea are completely destroyed without any change to the energy in sea. Neglecting the sea-swell coupling seems to be an acceptable approximation provided the sea's peak frequency remains higher than twice the peak frequency of the swell.

*B. Ocean Wave Directionality*

It is common in the oceanographic literature to see the 2D ocean wave spectrum written as the product of a one-dimensional frequency, or in this paper, wavenumber spectrum, $S(K)$, and a directionality function, $D(K,\phi)$,

$$\Sigma(K,\phi) = S(K) D(K,\phi). \tag{1}$$

In recent years, it has become more accepted that the directionality function of 2D wind-driven seas is generally bimodal and symmetric about the wind direction for frequencies above about twice the peak frequency. As summarized by Hwang et *al*. [9], earlier analysis of temporal measurements by wave-gauge arrays of directional buoys show unimodal directionality. Only recently, using maximum entropy and maximum likelihood signal processing methods, have bimodal features been extracted from temporal measurements. In contrast, a standard 2D Fourier transform procedure is sufficient to bring out the bimodal features from 3D topographical images. Ewans [10] has reported observations of the directional spectrum for fetch-limited seas, for the case of a well-defined 200 km fetch, showing a clear bimodal directional distribution. Ewans also found that the nondirectional spectrum associated with these fetch-limited seas conformed closely to the JONSWAP spectral shape, and the fetch dependencies of the parameters of the spectrum were quite similar to those observed in the JONSWAP experiment. A bimodal distribution has been previously observed from aerial stereo photography [9]. However the data quality of these earlier stereo photographs was not very high. As stated by Wang and Huang [11], numerical wave models have shown that the presence of a bimodal directional spreading is a robust feature at wavenumbers above the spectral peak. Recently, Huang et al. [2], [9], [11] used high resolution data from airborne scanning laser ranging system and GPS (Global Positioning System) technology, to

acquire 3D spatial topography of ocean surface waves during a quasi-equilibrium wind wave condition. From the spatial data, wavenumber spectra were computed directly. They concluded that for spatial components of the wave spectrum less than about twice the peak wavenumber, the distribution is unimodal. At higher wavenumbers, the spectrum becomes bimodal, more precisely, a bimodal distribution of the first kind, forming two lobes symmetric to the direction of the dominant wave, which for mature seas (long fetch) is coincident with the wind direction. On the other hand, Walsh [12] found that the peak of the spectrum is not in the wind direction until fetch reaches at least 150 km. The bimodal directivity function given is expressed as a function of horizontal wavenumber $K$ and azimuthal angle $\phi = a\tan\left(K_y/K_x\right)$. Allowing $\pi \le \phi < -\pi$ and requiring $\int_{-\pi}^{\pi} D(K,\phi)d\phi = 1$,

$$D(K,\phi) = \frac{1}{\pi}\left[0.5 + \sum_{n=1}^{\infty} a_n(K)\cos(n\phi)\right] . \qquad (2)$$

As demonstrated by Wang and Hwang, only eight terms are necessary to adequately describe the distribution. The Fourier coefficients, $a_n(\hat{K})$, where $\hat{K} = K/K_{peak}$, are calculated using the approximation $a_n(\hat{K}) = C_{1n}\hat{K}^{C_{2n}}\exp\left(-\hat{K}^{C_{3n}}\right) + C_{4n}$, and the empirical coefficients $C_{1n}$, $C_{2n}$, $C_{3n}$, and $C_{4n}$ are provided in [13]. Fig. 1 shows the surface roughness spectra for developing 2D seas that assume bimodal and the more familiar, but less realistic, $\cos^2(\phi/2)$ azimuthal dependence. The JOSWAP spectrum is assumed as are winds of 8 m/s wind $(u_{10})$ for 4 hrs into the $\phi = 0^\circ$ or $K_x = K_y = 0$ direction.

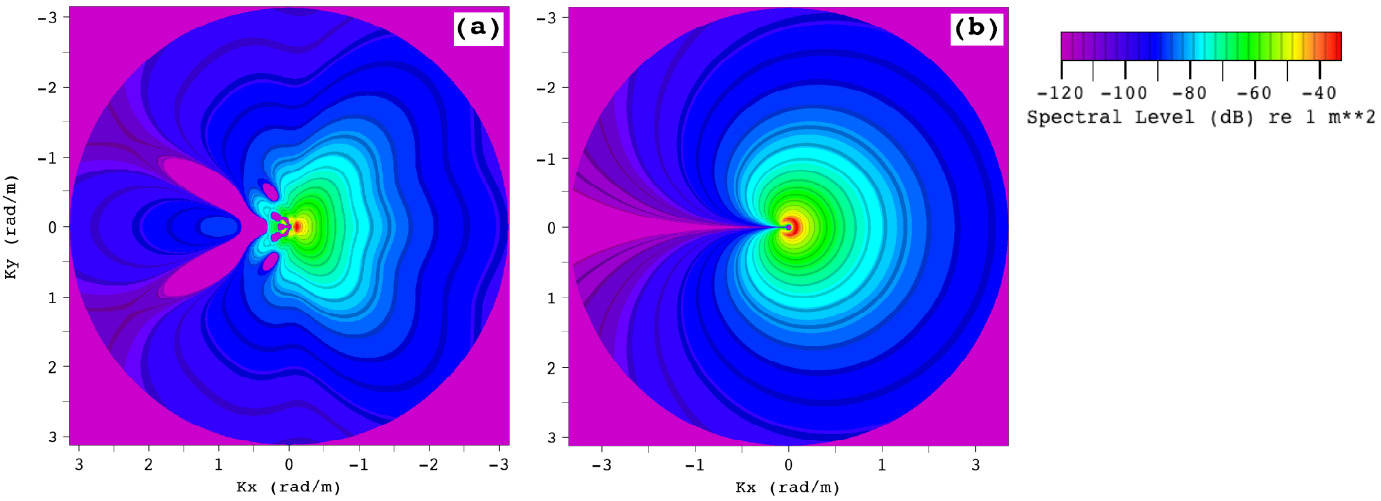


Fig. 1 Roughness spectra of 2D developing ocean waves assuming winds at 8 m/s for 4 hours. In (a) a bimodal distribution has been assumed and in (b) a cosine-squared azimuthal dependence has been assumed.

*A. Generating Deterministic Sea Surface Realizations*

The numerical surfaces used in this study are generated by linear filtering in the 2D wavenumber domain an array of random, uncorrelated numbers having unit variance and a Gaussian probability distribution function (PDF) of surface elevations. The transfer function of the linear filter is proportional to the square root of the 2D power spectrum of the surface elevations, $\Phi_M(K_x,K_y)$, which is derived from the wavenumber-angle representation, $\Phi_M(K,\phi)$ using $K = \sqrt{K_x^2 + K_y^2}$, $\phi = \arctan\left(K_y/K_x\right)$, and the Jacobian of the transformation, $(1/K)$. The time evolution of the surface realization is achieved by advancing in the wavenumber domain the phase of each $(K_x,K_y)$ component, according to its frequency, known through the dispersion relation $F = \pm\sqrt{gK}/2\pi$, and the desired time lag. This is by now a familiar process that has been thoroughly described in the literature of scattering from rough surfaces determined by stochastic process.

Based on the considerations identified in the previous section, the power spectra compatible with mixed seas are constructed under the following assumptions and approximations: First, the wind-driven component of the surface roughness is restricted to developing or growing seas (duration-limited). To avoid the bimodal directionality of the second kind, a phenomenon not modeled in the distribution function of Wang and Hwang, the fetch for the growing sea will be assumed to be larger than 150 km.

The non-directional part of the 2D spectrum is described by a JONSWAP spectrum [14], written here as a function of wavenumber:

$$S_J(K) = \frac{\alpha^*}{2} K^{-3} \exp\left[-\frac{5}{4}\left(\frac{K_m}{K}\right)^2\right] + Ln(\gamma)\exp\left[-\frac{1}{2\sigma^2}\left(\sqrt{\frac{K}{K_m}}-1\right)^2\right] \quad (3)$$

Here, $\gamma = 3.3$, $K_m = \left(49\pi^2\xi^{-0.66}\right)/g$, $\alpha^* = 0.076/\xi^{0.22}$, $\sigma = 0.07$ for $K \le K_m$ and $\sigma = 0.09$ for $K > K_m$, and $\xi = gT/u_{10}^{sea}$ where $T$ is the duration in seconds and $u_{10}^{sea}$ is the local wind speed at a height of 10 m. Second, the swell components of the mixed sea are assumed to be the remnants of a fully-developed sea generated at an earlier time or at a distant location and are represented by a truncated Pierson-Moskowitz spectrum [6]:

$$S_{PM}(K)dK = \frac{\alpha}{2} K^{-3} \exp\left[-\beta \frac{g^2}{K^2\left(0.92u_{10}^{swell}\right)^4}\right] dK \; . \quad (4)$$

And here, $\alpha = 0.0081$, $\beta = 0.74$, $u_{10}^{swell}$ is the wind speed that generated the swell measured at a height of 10 m, and only wavenumbers $K_{swell} < 1.01\, g/\left(u_{10}^{swell}\right)^2$ are allowed to contribute. The angular distribution function of Hwang and Wang is also applied to the swell spectrum, however, since the swell spectrum consists only of the low frequency band around the spectral peak, this distribution function reduces to a unimodal form. Third, the swell is assumed to propagate without damping. The modeling presented herein cannot be applied to shallow water environments where the ocean waves may be damped from shoaling. Fourth, the coupling between sea and swell is ignored. Following the assumption made in some hybrid wave models, depending on their relative spectral amplitudes the swell either dominates or disappears. To form the spectrum of the mixed sea $\Phi_M(K_x, K_y)$ containing sea and swell, the following logic is applied: At each point in the 2D wavenumber domain, the spectral amplitudes $\Phi_{sea}(K_x, K_y)$ and $\Phi_{swell}(K_x, K_y)$ are compared, if $\Phi_{swell} \ge \Phi_{sea}$, then $\Phi_M = \Phi_{swell} + \Phi_{sea}$, otherwise, $\Phi_M = \Phi_{sea}$.

## III. Modeling Acoustic Scattering for Moving Ocean Waves

In a recent paper [1], Keiffer et al. introduced and benchmarked an approach to modeling the acoustic Doppler from two-dimensional, time-evolving surfaces that started with the time-varying impulse response function. The method assumes a point source and works directly in the time domain so that the response of broadband signals can be naturally incorporated. It can also accommodate realistic source and receiver motion. The approach uses time-variant linear filter theory as a general framework and deals with the kinematics of the problem in the time domain where the time-varying impulse response of a moving interface is the fundamental quantity to be calculated. The impulse response of the time-evolving surface is calculated via the wedge assemblage (WA) model, which is based on the exact wedge diffraction solution of Biot and Tolstoy [15]. It is not limited by wave height, slope, or surface curvature. In [1], the methodology and validation for extending the WA model to scattering problems in which the surface, source, and receiver are in motion was presented. A systematic study was performed using a series of increasingly complicated moving surfaces. Space does not allow for a complete model description here. Any reader interested in a time domain methodology for accurately approximating the impulse response of surface or objects can find these details in Ref. [1].

### *A. Kinematics and the Single-Scatter Impulse Response*

Suppose that a moving (subsonic) point source, having instantaneous location $\bar{R}_S(t)$, stops at time $t = \tau$ and immediately begins injecting mass at a constant rate into a homogeneous (static) fluid medium [footnote]. The pressure impulse that radiates outward from the source travels (with speed $c$) from the location of the source at the time of emission and insonifies a moving (subsonic), impenetrable, rough surface, $z_s(x, y, t)$. As the impulsive source wave front sweeps across the time varying surface, it intercepts or detects each point on the surface at a discrete instant of time. This time of detection, $t_d$, solves the equation,

$$t_d - \tau - \left| x\hat{x} + y\hat{y} + z_s(x, y, t_d)\hat{z} - \bar{R}_S(\tau) \right| / c = 0 \; . \quad (5)$$

The locus of surface points detected by the impulsive source signal defines a new, effective surface, $\zeta(x, y, \tau)$, the frozen, quasi-static surface, $\zeta(x, y, \tau) = z_s(x, y, t = t_d)$.

Causality requires that the time history of the surface prior to the arrival of the incident impulse cannot affect the scattered response. Similarly, the single-scatter component of the scattered response cannot be affected by the time history of the surface after the initial source insonification. That is, the single-scatter component of the scattered response depends only on the shape of

the detected surface. The effect of source and surface motion on the time variation of the impulse response function can be modeled (in the single-scatter approximation) by examining the impulse responses of a time sequence of the quasi-static surfaces, $\zeta(x,y,\tau)$. Receiver motion can also be included. Regarding each point on the surface $\zeta(x,y,\tau)$ as a secondary source that emits a scattered impulse at $t=t_d$, let $t_R$ be the time at which that scattered signal reaches the moving receiver located at $t_R = t_d + \left| x\hat{x} + y\hat{y} + \zeta(x,y,\tau)\hat{z} - \bar{R}_R(t_R) \right| / c$. Each secondary source on $\zeta(x,y,\tau)$ emits a scattered impulse that reaches the moving receiver at a discrete, potentially different, future location. The effect of receiver motion can be included in the modeling by using the static effective receiver location in the impulse response calculation of each secondary source and then summing all the impulse responses with due respect to time of arrival.

*B. Numerical Implementation*

Although it is appropriate to repeat some of the details of a numerical implementation of the WA model here, the focus of this section is on the numerical implementation of the methodology being proposed to extend the WA model to time-variant problems. Begin by assuming that the time varying surface, $z_s(x,y,t)$, is represented on a fixed uniform spatial grid ($\Delta x = \Delta y$) and that the time evolution of the surface is known at all times. Then, at any discrete horizontal location, $(x_i, y_j)$, the value of the surface height function detected by the impulse emitted by the source at time $t=\tau$ defines $\zeta(x_i, y_j, \tau)$. Now, the surfaces of interest in this paper are modeled by filtering random numbers in the wavenumber domain and then Fourier transforming to the spatial domain. And the time evolution of the interface is accomplished by advancing in time the phase angle of different (wavenumber) spectral components at rates that are commensurate with the gravity wave dispersion relation $\Omega = \pm\sqrt{gK}$. To numerically determine the quasi-static surface $\zeta(x_i, y_j, \tau)$, the surface $z_s(x_i, y_j, t)$ is first generated at regular time intervals, $t_j = (j-1)\Delta T$. The height of the surface when the impulse from the source arrives is determined by interpolating between the two "snapshots" that bracket the solution to Eq. 5.

To calculate the (finite) impulse response of this surface using the WA method, the surface $\zeta(x_i, y_j, \tau)$ is "tiled" using triangularly shaped facets. These triangular facets are determined by first interpolating between any four surface heights of the square sample area to create a center surface height value. This divides the sample area into triangularly shaped pieces. Adjacent triangular facets are used to define finite-length wedge apices. The impulse response of the rough surface is modeled from the diffracted responses $(P_\delta)$ of every (non-shadowed) finite-length apex in the assemblage of wedges. The (finite) impulse response is calculated at discrete times, $t_i = (i-1)\Delta t$, using the exact solution of Biot and Tolstoy [16] and added with due respect to time of arrival:

$$\mathrm{h}(t_i, \tau) = \frac{1}{\Delta t} \sum_{m=1}^{M} \int_{t_i}^{t_i + \Delta t} P_{\delta_m}(\bar{r}_S, \bar{r}_R, t, \tau)\, dt \,. \qquad (6)$$

For a fixed source emission time $\tau$, sampling the impulse response function in time $t$, at interval $\Delta t$, determines, after Discrete Fourier Transform (DFT), a time-variant transfer function, $H(f_i, \tau)$, and (discrete) transform variable, $f_i$. $H(f_i, \tau)$ is defined on principal interval, $-f_{Nyq} \le f_i \le f_{Nyq}$, the highest frequency of which is the Nyquist frequency for the received frequency: $f_{Nyq} = 1/2\Delta t$. The finite extent of the rough surface ultimately limits the length of impulse response function and determines the received frequency resolution $\Delta f = 1/N\Delta t$. The discrete received frequencies are given by $f_i = -f_{Nyq} + (i-1)\Delta f$ where $i$ is a positive integer that is no greater than $N+1$. Based on past experience with static sinusoids and sea surfaces, choosing $\Delta t$ so that $f_{Nyq}$ is about an order of magnitude larger than the highest received frequency of interest $(f_{\max})$ is usually more than adequate.

Similarly, for a fixed reception frequency, $f_i$, sampling the transfer function $H(f_i, \tau)$ as it varies with source emission time $\tau$ ($M$ samples at interval $\Delta\tau$) introduces, after the corresponding DFT, another transform variable that can be identified as the discrete source frequency, $\upsilon_j = -\upsilon_{Nyq} + (j-1)\Delta\upsilon$. Here $j$ is a positive integer that is no greater than $M+1$. The discrete bifrequency function, $B(f_i, \upsilon_j)$, that results after this second DFT is specified in a two-dimensional frequency space over a rectangular-shaped principal band that is limited in one dimension by $-f_{Nyq} \le f_i \le f_{Nyq}$ and the other by $-\upsilon_{Nyq} \le \upsilon_j \le \upsilon_{Nyq}$. Here, the source Nyquist frequency, $\upsilon_{Nyq} = 1/2\Delta\tau$, should be large enough to satisfactorily minimize the "folding" of high frequency information down into the principal frequency band.

## *IV. Numerical Simulations*

In this section, frequency spectra of signals backscattered from different time-evolving, 2D seas are calculated, and presented in a series of increasingly complex and realistic ocean-acoustic simulations. In the first simulation, the azimuthal dependence of the frequency spectra of signals backscattered (30˚ grazing) from 2D seas that have assumed the bimodal distribution function are examined and, for reference, compared with simulations that assumed the $\cos^2(\phi/2)$ azimuthal dependence. In other numerical experiments, the grazing angle is lowered from 30˚ to 10˚, the effects of wind duration and swell-contamination are investigated. In all of these numerical experiments (unless specified otherwise), the simulated 2D sea surfaces were specified at discrete times on a finite-sized ( $Lx = Ly = 251.3\ m$ ) uniform grid ( $\Delta x = \Delta y = 0.245\ m$ ). Each time-evolving surface was examined for 30 s at 0. 2 s intervals. Ten realizations of the frequency spectrum of the backscattered signal were computed (one each from 10 realizations of a particular sea surface spectrum) and averaged. The average frequency spectrum is plotted, more accurately, $10 \cdot Log_{10}\left(16\pi^2 (r_R + r_S)^2 \left\langle P_{out}(\eta) P_{out}^*(\eta) \right\rangle\right)$ is plotted. Here $\eta = f - \upsilon$ is the Doppler shift, $f$ is the received frequency, and $\upsilon$ is the source frequency (10 Hz to 330 Hz). The factor $16\pi^2 (r_R + r_S)^2$ comes from the normalization of the scattered time signal by the magnitude of the corresponding image reflection.

### *A. Bimodal versus Cosine-Squared Directionality*

To examine the impact that a bimodal dependence for the ocean waves may has on the acoustic scattering, the azimuthal dependence of the average (monostatic) backscattered frequency spectrum was calculated for developing 2D seas due to an 8 m/s wind $(u_{10})$ that persisted for 4 hrs into the $\phi = 0^\circ$ direction (see Fig. 1). These calculations were carried out for the bimodal and cosine-squared spectra for six azimuthal angles: 0˚, 15˚, 30˚, 45˚, 60˚, and 90˚ (crosswind). Note that an azimuthal angle of $\phi = 0^\circ$ corresponds to case of backscattering from seas whose dominant direction (identical to the wind direction for wavenumbers $K < 2K_{peak}$ ) is toward the source/receiver location. The source and receiver remained fixed in these experiments so an azimuthal angle of $\phi = 90^\circ$ corresponds to case of backscattering from seas whose dominant direction is perpendicular to the incident/scattered direction. For azimuthal backscatter angles 0˚, 15˚, 30˚, 45˚, Fig. 2 shows, respectively, the average backscattered frequency spectra (Doppler Spectrum). Fig 3. shows the Doppler Spectrum for azimuthal orientation of 60˚, and 90˚. The color bar in Fig. 3 applies to Fig. 2 as well. In all cases, the nominal grazing angle is 30˚. Certainly the most noticeable differences between the two sets of results are in the down-shifted parts of the Doppler spectra. These contributions to the received spectrum are due to ocean wave components that are traveling away from the source/receiver location. From the bimodal roughness spectra in Fig. 1, it can be seen that for wavenumbers less than about 2. 0 rad/m, there are prominent "holes" in the $K_y < 0$ part of the roughness spectrum. It can also be noted that under the bimodal assumption, there is clear acoustic evidence in the $\phi = 0^\circ$ geometry of ocean wave components traveling against the wind. In contrast, and as expected, the cosine-squared distribution function yields a backscattered frequency spectrum that shows no evidence of ocean waves traveling away from the source/receiver location. For the $\cos^2(\phi/2)$ directionality function, the first evidence of down-shifted contributions begin with the $\phi = 15^\circ$ orientation.

Other features of the results worth noting are: 1) The very weak scattered response for source frequencies below about 11 Hz, evident for both azimuthal models that is due to the lack of ocean wave energy at the long wavelengths. 2) The spreading about the spectral peak is not symmetric. When there is a dominant up or down-shifted Bragg-scale ocean wave component, the backscattered spectrum tends to spread toward Doppler shifts that are higher than the Bragg-shift. When the azimuthal orientation is such that there are comparable Bragg-scale ocean wave components traveling both toward and away from the source/receiver direction (say from $\phi = 75^\circ$ and greater) then the spreading about the Bragg component tends to slightly favor Doppler shifts that are lower than the expected Bragg-shift. 3) For source frequencies below about 100 Hz, it can be see that the combination of significant ocean wave energy moving both toward and away from the source/receiver leads to scattering contributions that fall into unshifted ( $\eta = 0$ Hz) Doppler band.

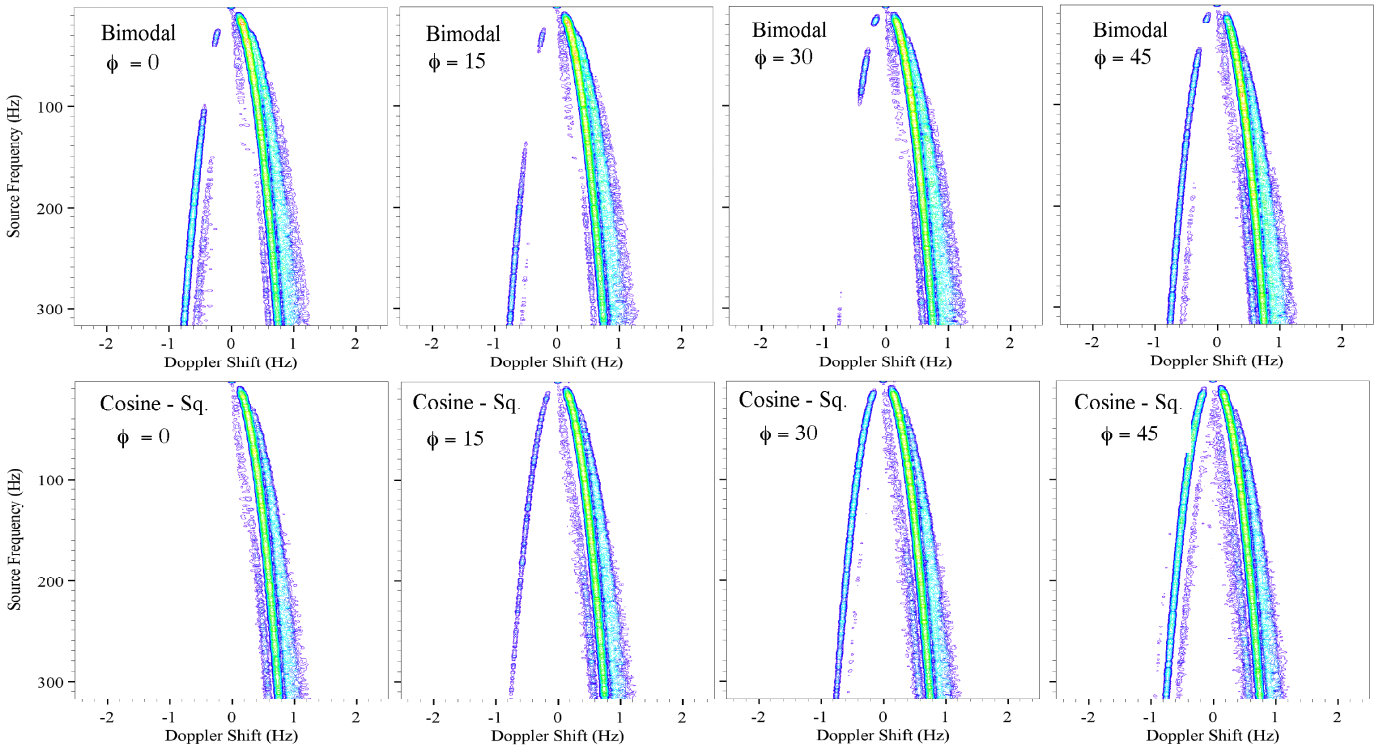


Figure 2: Azimuthal dependence of monostatic backscatter Doppler spectrum from seas having a bimodal and cosine – squared distributions. Grazing angle is 30˚ and azimuthal angles are: 0˚, 15˚, 30˚, 45˚.

*B. Wind Duration*

As is well known, when a (constant, uniform) wind starts blowing on the ocean surface the short wavelength components of the ocean wave spectrum are quickly established and then saturated. As the wind continues to blow, longer and longer wavelength components become energized, the peak of the ocean wave spectrum moves to lower wavenumbers, and the overall roughness of the air sea interface increases. This suggests that there would be little change to the Doppler spectrum in a backscatter geometry for source frequencies above several tens of Hz. Two obvious caveats come to mind: First, unlike the cosine-squared distribution function, the bimodal distribution function depends on the wavenumber where the ocean wave spectrum peaks. Second, the importance of non-Bragg scattering (i. e. , scattering contributions not described by the first order term of the perturbation theory) will increase/decrease with increasing/decreasing ocean wave roughness. Simulation results for the average backscattered Doppler spectrum (30˚ grazing and 0˚ azimuth) from an a ocean wave field due to an 8 m/s wind but having a duration of only 1 hr are shown in Figure 4a. To facilitate the comparison, the 30˚ grazing and 0˚ azimuth calculation belonging to Fig. 1 (8m/s and 4 hr duration) is reproduced in Figure 4b on a somewhat larger scale.

Looking at Figure 4, it can be seen that when the duration of the wind is shortened the peak in the scattered response moves to a higher source frequency (40 Hz up from 20 Hz for the 4 hour duration case). The change in the bimodal distribution caused by the change in the wind duration can be clearly seen by comparing the down-shifted part of the Doppler spectrum. In Figure 4b, the absence of significant long wave energy makes more distinct the “turning on” (at a source frequency of about 60 Hz and again at 150 Hz) of the higher order scattering effects that create the first and second shoulders to the right (greater Doppler Shifts) of the up-shifted Bragg branch. Note that these shoulders also occur in the plot for the 4 hour duration seas but emerge at lower source frequencies (30 and 90 Hz) and with such a smaller separation in Doppler shift from the main Bragg branch.

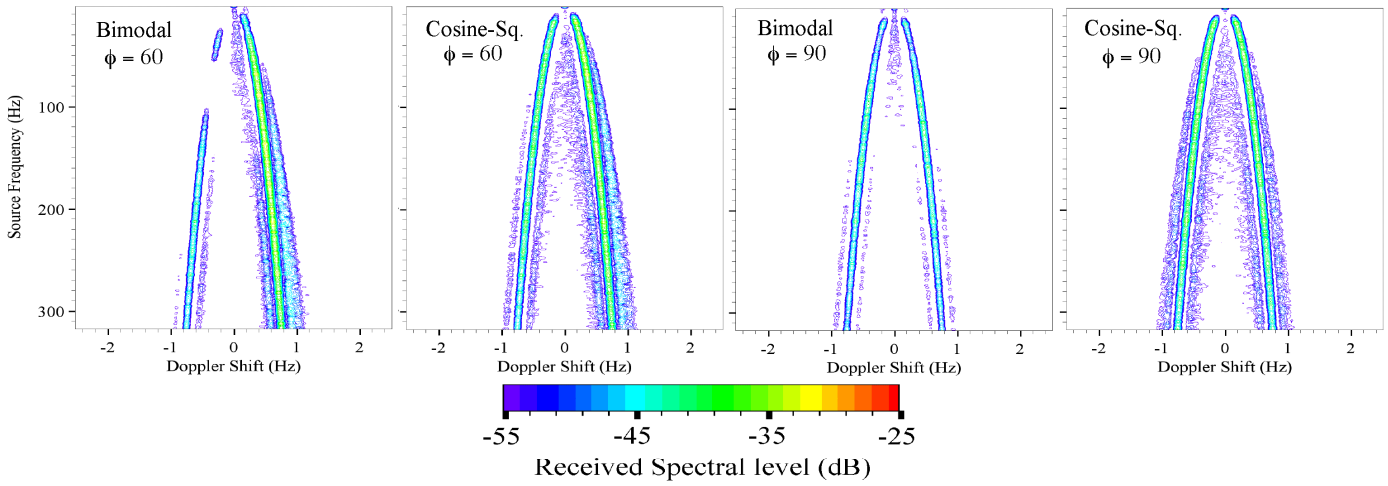


Figure 3: Azimuthal dependence of monostatic backscatter Doppler spectrum from seas having a bimodal and cosine – squared distributions. Grazing angle is 30˚ and azimuthal angles are: 60˚ and 90˚ (cross-wind).

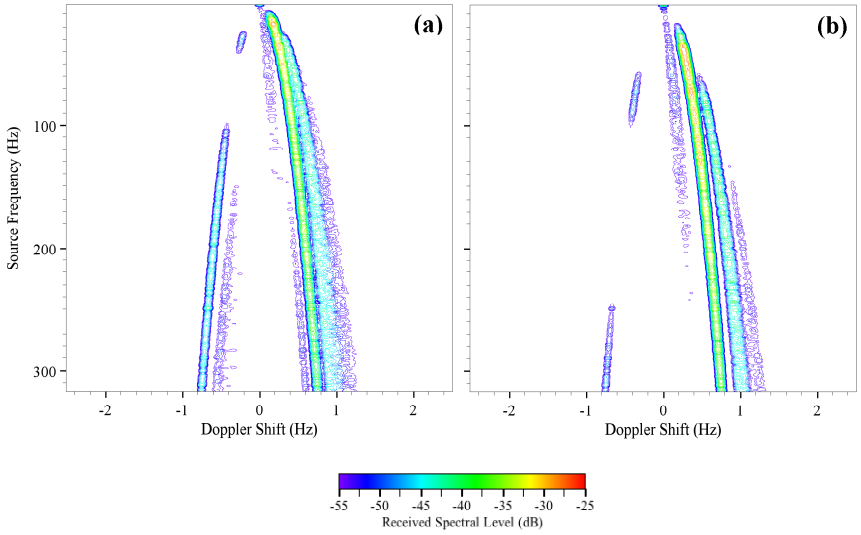


Figure 4: Effect of wind duration on Doppler spectrum assuming bimodal seas: (a) wind duration = 8 hrs, (b) wind duration = 1 hr.

C. *Swell Contamination*

As stated in the opening paragraphs of this paper, the common situation encountered during an acoustics experiment is that of a mixed sea. The presence of swell obviously contributes energy to the low wavenumber part of the ocean wave spectrum that, in moderate grazing angle backscatter geometries, should make available first order or Bragg-scale scattering contributions at correspondingly very low source frequencies (perhaps less than 20 Hz). The question more apropos of the typical at-sea experiment is how does the presence of the swell affect the Doppler spectrum at higher source frequencies? The scenario studied next begins with the wind blowing constantly at 14 m/s for many hours into the $\phi = 180^{\circ}$ direction and then suddenly decreasing to 8 m/s and changes direction to the $\phi = 0^{\circ}$ direction. Figure 5 shows the average Doppler spectrum that that results 1 hr after this new wind direction is established. Here the source/receiver grazing angle is again 30˚ with azimuthal orientation $\phi = 0^{\circ}$.

For reference, this result is compared to Figure 4b because it shares the same instantaneous wind conditions and scattering geometry.

From Figures 5 it can be seen that the swell contributes to the acoustic response near a source frequency near 5 Hz. At slightly higher source frequencies, between 10 – 20 Hz, there is a drop-out in the scattered response because the swell cuts-off and the duration of the new wind is too short to generate significant ocean waves at the long wavelengths needed for Bragg scattering at 10 – 20 Hz. Above a source frequency of 20 Hz the scattering picks up again as the longest ocean waves associated with the new wind direction begin to supply significant Bragg-scale roughness. The presence of the long swell waves increases the overall roughness of the surface and this causes the "turning on" of the higher order scattering contributions at lower source frequencies. The distinct shoulders, so clearly seen in Doppler spectrum shown in Fig. 4, are now smeared out because the higher order contributions that involve both the long waves of the swell and Bragg scale components of the sea have Doppler shifts that are only slightly different from the Doppler shifts associated with the Bragg scale components. Finally, it can be seen that the direction of the swell changes the spreading about the Doppler peak. In this case, the spreading is symmetric about the peak shift.

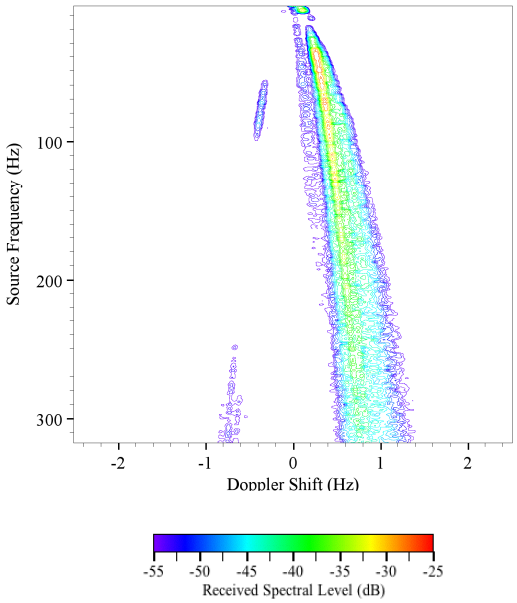


Figure 5: Effect of swell contamination on monostatic backscatter Doppler spectrum. Swell due to 14 m/s wind added to seas driven by 8 m/s wind for 1 hour.

.

## ACKNOWLEDGEMENT

The author thanks and acknowledges the many useful technical conversations and earlier contributions regarding ocean wave modeling that he has enjoyed with Dr. Jorge Novarini of the Naval Oceanographic Office. This document, NRL/MM/7180-08-0082, has been reviewed and is approved for public release.

## REFERENCES

[1] R. S. Keiffer, J. C. Novarini, and R. W. Scharstein, "A Time-Variant Impulse Response Method for Acoustic Scattering from Moving Two-Dimensional Surfaces," J. Acoust. Soc. Am., 118, 1283-1299, (2005).

[2] P. A. Hwang, D. W. Wang, E. J. Walsh, W. B. Krabill, and R. N. Swift, "Airborne Measurements of the Wavenumber Spectra of Ocean Surface Waves. Part II: Directional Distribution," J. Phys. Ocean., 30, 2768-2787, (2000).

[3] R. S. Keiffer, J. C. Novarini, and G. V. Norton, "The Impact of the Background Bubble Layer on Reverberation-Derived Scattering Strengths in the Low to Moderate Frequency Range," J. Acoust. Soc. Am., 97, 227-234, (1995).

[4] D. W. Wang, and P. A. Hwang, "An Operational Method for Separating Wind Sea and Swell from Ocean Wave Spectra," J. of Atmospheric and Oceanic Tech., 18, 2052-2062, (2001).

[5] I. R. Young, *Wind Generated Ocean Waves*, Elsevier (1999).

[6] W. J. Pierson and L. Moskowitz, “A Proposed Spectral Form for Fully Developed Wind Seas Based on the Similarity Theory of S. A. Kitagorodskii,” J. Geophys. Res., 69, 5181-5190, (1964).

[7] G. Chen and S. E. Becher, “Effects of long Waves on Wind-Generated Waves,” J. Phys. Oceanogr,, 30, 2246-2257(1999).

[8] “Ocean Wave Modeling” (The SWAMP group) Plenum Press (1985).

[9] P. A. Hwang, D. W. Wang, E. J. Walsh, W. B. Krabill, and R. N. Swift, ”Airborne Measurements of the Wavenumber Spectra of Ocean Surface Waves. Part I: Spectral Slope of the Wavenumber Spectra of Ocean Waves,” J. Phys. Oceanogr., 30, 2753-2767, (2001).

[10] K. C. Ewans, “Observations of the Directional Spectrum of Fetch-Limited Waves,” J. Phys. Oceanogr. 28, 495-512, (1998).

[11] D. W. Wang and P. A. Wang, ”Evolution of the Bimodal Directional Distribution of Ocean Waves,” J. Phys. Oceanogr. , 31, 1200-1221, (2001).

[12] E. J. Walsh, D. W. Hancock III, D. E. Hines, R. N. Swift, and J. F. Scott, “An Observation of the Directional Wave Spectrum Evolution from Shoreline to Fully Developed,” J. Phys. Oceanogr., 19, 670-690, (1989).

[13] D. W. Wang and P. A. Hwang, ’Higher Fourier harmonics of the directional distribution of an equilibrium wave field under steady wind forcing,” J. Atmosph. and Oceanic. Tech., 20, 217-227, (2003).

[14] K. D. Hasselmann, W. Sell, D. B. Ross, and P. Muler, “A Parametric Wave Prediction Model,” J. Phys. Oceanogr., 6, 200-228, (1976).

[15] M. A. Biot and I. Tolstoy, "Formulation of Wave Propagation in Infinite Media by Normal Coordinates with Application to Diffraction," J. Acoust. Soc. Am., 29, 381-391, (1957).